

Heterogeneous Catalysis

How to cite: *Angew. Chem. Int. Ed.* **2020**, 59, 18686–18694

International Edition: doi.org/10.1002/anie.202007790

German Edition: doi.org/10.1002/ange.202007790

Rigid Arrangements of Ionic Charge in Zeolite Frameworks Conferred by Specific Aluminum Distributions Preferentially Stabilize Alkanol Dehydration Transition States

Alexander J. Hoffman, Jason S. Bates, John R. Di Iorio, Steven V. Nystrom, Claire T. Nimlos, Rajamani Gounder,* and David Hibbitts*

Abstract: Zeolite reactivity depends on the solvating environments of their micropores and the proximity of their Brønsted acid sites. Turnover rates (per H^+) for methanol and ethanol dehydration increase with the fraction of H^+ sites sharing six-membered rings of chabazite (CHA) zeolites. Density functional theory (DFT) shows that activation barriers vary widely with the number and arrangement of Al (1–5 per 36 T-site unit cell), but cannot be described solely by Al–Al distance or density. Certain Al distributions yield rigid arrangements of anionic charge that stabilize cationic intermediates and transition states via H-bonding to decrease barriers. This is a key feature of acid catalysis in zeolite solvents, which lack the isotropy of liquid solvents. The sensitivity of polar transition states to specific arrangements of charge in their solvating environments and the ability to position such charges in zeolite lattices with increasing precision herald rich catalytic diversity among zeolites of varying Al arrangement.

Introduction

Zeolites are crystalline aluminosilicates that are ubiquitous as acid catalysts in carbon conversion routes^[1,2] because they provide diversity of function arising from differences in crystal topology and habit, which can be synthetically engineered.^[3–7] Their microporous voids are of molecular dimension (< 2 nm) and provide solvating environments that confine and stabilize, via non-specific van der Waals interactions, the covalent and ion-pair intermediates and transition states that mediate gas-phase reactions.^[8–11] Zeolite micropores also contain Brønsted acidic OH groups that charge-compensate framework Al and Si-OH groups at lattice defects which act as hydrophilic binding sites that influence the extended H-bonded clusters of water,^[12] alkanols and other polar protic molecules commonly used as solvents in liquid-phase reactions.^[13–17] Absent a condensed intrapore

phase, however, catalytic regimes exist wherein molecular clusters and networks of specific structure and size are stabilized at Brønsted acid sites within microporous voids, and their stability depends intimately on the geometry and charge distribution within the environment provided by the solvating zeolite lattice.^[18] Such features of the zeolite “solvent” and their effects on acid catalysis, however, are not well understood.

Additionally, the effects of zeolite acid site proximity on turnover rates have been documented,^[19,20] but only anecdotally and with little understanding or consensus about the mechanistic origin of such rate differences. Acid strength—as determined by deprotonation energy (DPE), a theoretical metric defined as the energy to remove a proton from its conjugate base to a non-interacting distance—increases for Brønsted acid sites in proximal configurations (Al-O-(Si-O)_x-Al, $x = 1, 2$),^[21] indicating that interactions between proximal sites may increase turnover rates solely due to electronic effects by facilitating charge separation during transition state formation.^[22,23] Turnover rates of protolytic alkane activation^[24] and alkene oligomerization^[25–27] are reported to increase with acid site proximity in MFI zeolites, yet firm mechanistic interpretations are precluded by the numerous Al-Al pair configurations present within the low-symmetry (12 tetrahedral-site; T-site) MFI framework. Here, we examine the effects of acid site proximity in zeolite catalysis using the high-symmetry (1 T-site) CHA framework and alkanol dehydration as the probe reaction, which offers significant promise for developing mechanistic understanding of how acid site proximity influences turnover rates, given that the abundant surface intermediates and reaction mechanisms in this chemistry are well understood.^[28] Moreover, gas-phase alkanol dehydration reactions can occur at high coverages of adsorbed alkanol clusters and networks reminiscent of those present during liquid-phase catalysis, promising to offer molecular insight into interactions among proximal acid sites mediated by co-adsorbates that have gone largely ignored in prior studies of H-form zeolites, but constitute a mechanism by which turnover rates vary with site arrangement.

Results and Discussion

SSZ-13 zeolites (CHA, Figure 1) have one crystallographically unique T-site; as such, each acid site has an identical local environment, thus avoiding complications of different

[*] A. J. Hoffman, Dr. S. V. Nystrom, Prof. Dr. D. Hibbitts
Department of Chemical Engineering, University of Florida
1030 Center Dr, Gainesville, FL 32608 (USA)
E-mail: hibbitts@che.ufl.edu

Dr. J. S. Bates, Dr. J. R. Di Iorio, C. T. Nimlos, Prof. Dr. R. Gounder
Charles D. Davidson School of Chemical Engineering, Purdue
University
480 Stadium Mall Drive, West Lafayette, IN 47907 (USA)
E-mail: rgounder@purdue.edu

Supporting information and the ORCID identification number(s) for the author(s) of this article can be found under:
<https://doi.org/10.1002/anie.202007790>.

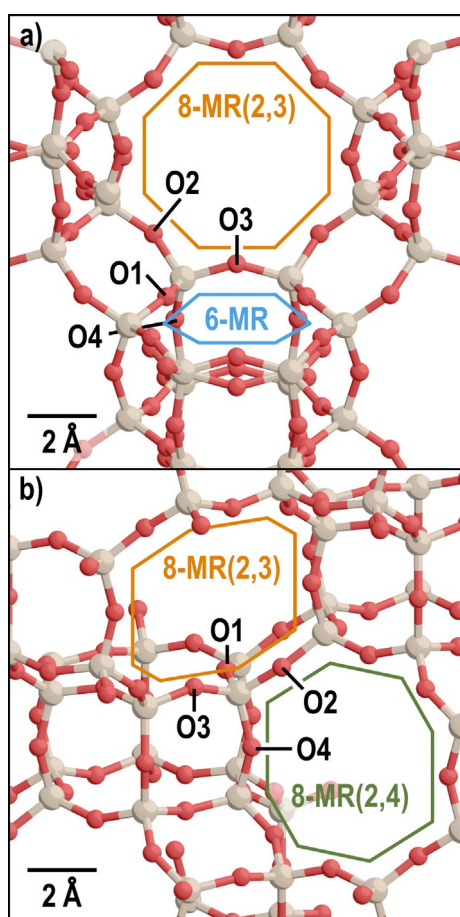


Figure 1. The CHA structure showing a) the 6-MR and 8-MR(2,3) (containing O2 and O3) structures and b) the 8-MR(2,3) and 8-MR(2,4) around one T-site. The four symmetric O atoms around one T-site are labelled.

acid site locations and reducing the combinatorial complexity of proximal Al-Al site ensembles. CHA is comprised of 6-membered ring (6-MR) units adjacent to 8-MR windows (3.7 Å in diam.) that separate CHA cages (7.4 × 9.8 Å).^[29] CHA can be synthesized with a specific acid site density (Si:Al ratio) but with varying distributions of proximal Al-Al site ensembles, for example by varying the ratios of *N,N,N*-trimethyl-1-adamantylammonium (TMAda⁺) to Na⁺ structure-directing agents (SDAs) present during crystallization at fixed total SDA cation concentration.^[30,31] This synthesis procedure enables systematically varying the number of Al-Al pairs within a 6-MR (as measured by Co²⁺ titration^[30,32]), thus avoiding effects caused by simultaneously varying bulk acid site density to allow better elucidation of acid site proximity effects on catalysis.^[24,25,33,34] This and other methods to influence Al proximity in zeolites^[20,26,35,36] have motivated renewed investigation of the kinetic and mechanistic consequences of acid site proximity in zeolite catalysis.^[19]

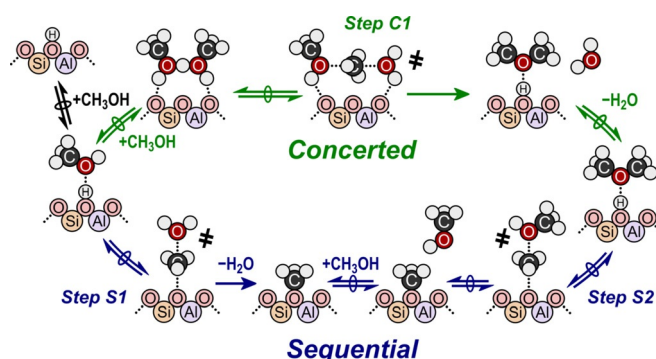
Methanol dehydration to dimethyl ether (DME) is an informative probe reaction for solid Brønsted acids, used previously to decouple acid strength and confinement effects among zeolites of different acid strength and topology^[22,23,37–40] and polyoxometalates.^[23,41,42] Methanol dehydra-

tion can occur by two competing mechanisms: a sequential (dissociative) or a concerted (associative) mechanism (Scheme 1), where the former creates a surface methyl (CH₃-Z) that reacts with methanol to form DME, while the latter forms DME in a single bimolecular reaction. At 415 K, a typical reaction condition, density functional theory (DFT) calculations show that methanol dehydrates via the concerted mechanism at all relevant methanol pressures (> 0.3 kPa) in CHA.^[28] Abundant surface species vary from methanol monomers to dimers and larger methanol clusters over the pressure ranges of kinetic studies, and their change in molecularity causes a transition from a first- to a zero-order regime on all H-form zeolites.^[22,28,37,43] With increasing methanol pressure, rates become inhibited by CH₃OH on small-pore, cage-window zeolites (CHA, AEI, LEV, LTA; structures shown in Figures S1–S3, SI) because methanol clusters (≥ 3 CH₃OH per H⁺) larger than the molecularity of kinetically relevant transition states form, requiring desorption of some extraneous methanol prior to reaction.^[28,32] Such methanol dehydration rates are described by:

$$r_{\text{DME}} = \frac{k_{\text{first}} P_{\text{M}}}{1 + \frac{k_{\text{first}}}{k_{\text{zero}}} P_{\text{M}} + \frac{k_{\text{first}}}{k_{\text{inhib}}} P_{\text{M}}^2} \quad (1)$$

where k_{first} , k_{zero} , and k_{inhib} are the first-order, zero-order, and inhibitory rate coefficients and P_{M} is the methanol pressure (derivation in Section S9, SI).^[28,32]

Recently, we reported that methanol dehydration turnover rates (per H⁺) increase systematically with the percentage of 6-MR paired acid sites in H-CHA (0–44%; Figure 2).^[32] First- and zero-order rate coefficients [Eq. (1)] fit to the kinetic data also increase systematically with site-pairing in the 6-MR, and rate constants extrapolated to a hypothetical CHA sample with 100% of its sites in paired configurations (Figure 2) are 7.2 × and 4.4 × larger for first-order and zero-order rate coefficients, respectively, than on isolated sites.^[32] The first-order rate coefficient reflects the effective free energy barrier (ΔG^\ddagger) to form a transition state with one additional methanol from an adsorbed methanol complex (e.g., forming a bimolecular transition state from a methanol monomer).^[23,28] The zero-order rate coefficient instead re-



Scheme 1. Two parallel methanol dehydration mechanisms: concerted (top) and sequential (bottom). Both routes can occur with spectating methanol molecules forming extended complexes with the species depicted; adapted from prior work.^[28]

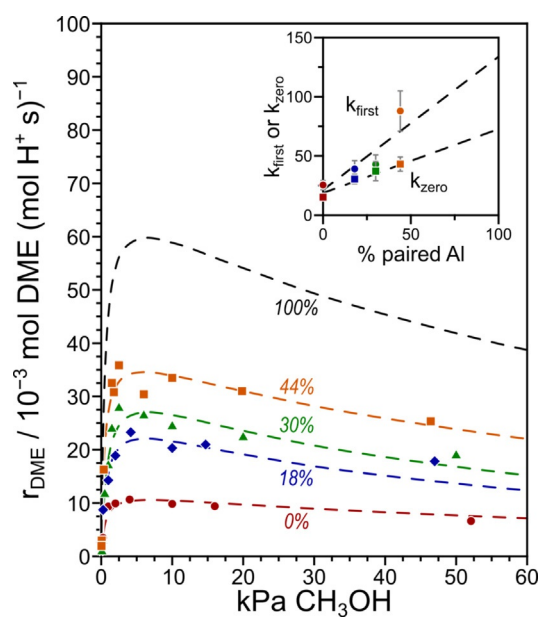


Figure 2. DME formation rates (per H^+ , 415 K) as a function of methanol pressure on H-CHA with 0% (●, red), 18% (◆, blue), 30% (▲, green), 44% (■, orange), and the extrapolation to 100% (black) 6-MR paired Al. Dashed lines represent regression to Equation (1). Inset: first-order (k_{first} , ●, 10^{-3} mol DME ($\text{kPa mol H}^+ \text{s}^{-1}$) and zero-order (k_{zero} , ■, 10^{-3} mol DME ($\text{mol H}^+ \text{s}^{-1}$) rate coefficients as a function of the percentage of 6-MR paired Al. Adapted from prior work.^[32]

flects the intrinsic activation free energy (ΔG_{act}) to form a transition state with the same number of methanol molecules as its precursor (e.g., forming a bimolecular transition state from an adsorbed methanol dimer).^[23,28] The higher rate coefficients on paired sites correspond to apparent and intrinsic free energy barriers (ΔG^\ddagger and ΔG_{act}) values that are lower by 7 and 5 kJ mol^{-1} , respectively, on paired than on isolated sites. Transition states can be unimolecular, bimolecular, or have additional H-bonded methanol molecules that act to stabilize them; similarly, adsorbed methanol complexes can include 1–4 methanol molecules over this range of methanol pressures (0.15–52 kPa).^[28]

There are three possible Brønsted acid site-pair locations within the 6-MR (*AC*, *AD*, *AE*, Figure 3), omitting pairs in which Al occupy neighboring T-sites that would violate Löwenstein's Rule.^[44] The Al in both the *AC* and *AE* site-pairs are separated by one Si atom (Figure 3 a,b), forming two next-nearest neighbor (NNN) site-pairs. These arrangements behave as a single indistinguishable site-type during catalysis (see Section S4, SI), and thus are treated collectively. The Al in the *AD* site-pair are separated by two Si atoms and are thus in next-next-nearest neighbor (NNNN) positions (Figure 3 c). Acid sites in these 6-MR paired configurations are stronger acids because deprotonation of one site in the pair allows the other proton to H-bond with and stabilize the conjugate base (Figure 3),^[21] evident in decreases in DPE of 19 and 15 kJ mol^{-1} for the *AC* (NNN) and *AD* (NNNN) site-pairs, respectively, compared to an isolated site. In contrast, the *AE* site-pair does not allow the framework to contort upon deprotonation of the *A* site to facilitate the O1-H-AlO_4^-

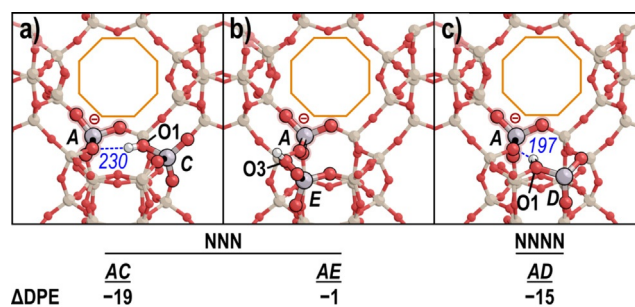


Figure 3. Change in acid strength relative to an isolated site, given by the DPE difference (kJ mol^{-1}). The conjugate base upon A-site deprotonation is shown for the NNN site-pairs a) *AC* and b) *AE*, and the NNNN site-pair c) *AD*. Blue dashed lines represent H-bonds (lengths in pm). Adapted from prior work.^[21]

interaction (Figure S5, SI); instead, the remaining proton on site *E* binds to *O3*, precluding H-bonding to the conjugate base and resulting in the same DPE as an isolated site ($\Delta\text{DPE} = -1$ kJ mol^{-1} , Figure 3b). These calculations show that H-bonding can stabilize conjugate bases across 6-MR motifs in both NNN and NNNN Al site-pair arrangements; importantly, they reveal how cationic species (here, a proton) are stabilized by specific arrangements of Al and associated anionic charge positioned in the solvating environment.

These interactions between a conjugate base and a bare proximal proton may be relevant to reactions that prevail at low acid site coverages, such as high-temperature (> 700 K) alkane cracking.^[9,33,45–52] Methanol dehydration, however, occurs at acid sites that are fully covered by methanol species (> 0.15 kPa CH_3OH ; in situ IR^[28,32] and DFT^[28] evidence). Co-adsorbed methanol species alter the H-bonding interactions among site-pairs that determine DPE and influence the stability of methanol dehydration transition states. Thus, we performed a theoretical evaluation of methanol dehydration at isolated and paired Al in CHA to elucidate the mechanistic origins of the observed rate enhancement.

Methanol dehydration reactions were modeled at site *A* while the second site (*C*, *D*, *E*) binds spectating molecules. We focus on reactions with 1–2 adsorbed CH_3OH per site (results with bare proximal sites in Section S5, SI), and the simplest routes that form DME (sequential and concerted paths without spectators) because these capture barriers for CH_3OH adsorption to form a protonated dimer and then to form DME, which are the dominant factors affecting turnover rates. These methanol dehydration routes involve three transition states (Scheme 1) corresponding to zeolite methylation (Step S1), methanol methylation (Step S2), and concerted DME formation (Step C1).^[28] The free energies and structures presented here for reactants and transition states are the most stable among ~ 150 unique optimized structures for each reaction that were identified by altering the framework O atoms involved in methylation/demethylation reactions and by systematic reorientations of exemplars. These reorientations (described in Section S6, SI) are necessary because DFT methods only identify reactants and transition states near input structures, while numerous structures exist differing in energy by up to 200 kJ mol^{-1} .^[53]

Reorientations indicate that H-bonding is critical for these transition states; configurations that maximize H-bonding with minimal framework restructuring and internal transition state distortions are consistently preferred.

We first examine the most stable transition states at isolated Al (*A*) sites (Figure 4a–c). Zeolite methylation (Step S1) has a transition state structure of $\text{H}_2\text{O}-\text{CH}_3^+-\text{O}_z^-$ and is most stable within 8-MR(2,3) with H_2O forming two H-bonds with framework O atoms (Figure 4a); it has an intrinsic activation barrier (ΔG_{act} , 415 K, 1 bar) of 135 kJ mol^{-1} when methylating O3. The transition state for methanol methylation (Step S2) is nearly identical with CH_3OH instead of H_2O

($\text{CH}_3\text{OH}-\text{CH}_3^+-\text{O}_z^-$) and one H-bond with the framework; it prefers demethylating O4 and has a ΔG_{act} of 78 kJ mol^{-1} (Figure 4b). The transition state of the concerted reaction (Step C1, $\text{CH}_3\text{OH}-\text{CH}_3^+-\text{H}_2\text{O}$) resides in the CHA cage and H-bonds to two O of the conjugate base in 8-MR(2,4) (Figure 4c); it has a ΔG_{act} of 138 kJ mol^{-1} and an effective barrier (ΔG^\ddagger) of 123 kJ mol^{-1} , referenced to an adsorbed methanol monomer that is the most abundant surface intermediate (MASI) at low methanol pressure. This ΔG^\ddagger for concerted DME formation (123 kJ mol^{-1}) is 12 kJ mol^{-1} lower than that of zeolite methylation (Step S1, $\Delta G^\ddagger = 135 \text{ kJ mol}^{-1}$), which limits the rate of the sequential pathway. The lower barrier for the concerted mechanism indicates that it prevails over the sequential pathway at isolated acid sites and at conditions relevant to kinetic studies, as shown in our prior work.^[28]

We next examine the most stable transition states at paired Al sites in NNN positions (*AC*), where the second site has one adsorbed methanol (Figure 4d–f). Step S1 transition states are most stable in the 8-MR(2,4) to avoid interacting with the methanol bound to site *C*. This methanol facilitates an interaction between the proximal Al sites through two strong H-bonds (129 and 166 pm) that reduce the ΔG_{act} for surface methylation to 131 kJ mol^{-1} on the NNN site-pair (Figure 4d) from 135 kJ mol^{-1} on an isolated site (Figure 4a). Adding the second site decreases the barrier by 17 kJ mol^{-1} for methylating in 8-MR(2,4), but rearranging the transition state from 8-MR(2,3) to 8-MR(2,4) requires $+13 \text{ kJ mol}^{-1}$, resulting in an effective decrease of 4 kJ mol^{-1} (Figure S9, SI). An analogous interaction exists for Step S2 (Figure 4b,e) and decreases ΔG^\ddagger by 14 kJ mol^{-1} on the NNN site-pair compared to the isolated Al site, although this step is not kinetically relevant during methanol dehydration.^[28,32] Concerted methanol dehydration also occurs with lower ΔG^\ddagger and ΔG_{act} on the NNN site-pair (118 and 127 kJ mol^{-1}) than on isolated sites (123 and 138 kJ mol^{-1} ; Figure 5), and this pathway should thus prevail over the sequential pathway at these conditions.^[28] These reductions of 5 and 11 kJ mol^{-1} in ΔG^\ddagger and ΔG_{act} , respectively, for the concerted methanol pathway are similar to the decrease in free energy barriers (7 and 5 kJ mol^{-1}) measured in experimental kinetic data.^[32] All three methanol dehydration transition states are stabilized by the presence of a methanol monomer associated with a second Al site at the NNN position in the 6-MR, indicating that alkanol co-adsorbates facilitate inter-site H-bonding interactions similar to how bare protons do so to increase acid strength (Figure 3), rather than stabilizing transition states via van der Waals interactions. These differences in free energy barriers of 4 – 15 kJ mol^{-1} are consistent with the observed rate increases but are relatively small compared to the overall accuracy of DFT methods, so a second site-pair (NNNN) can corroborate these findings.

We also examine the most stable transition states at paired Al sites in NNNN positions (*AD*) to determine whether these decreases in free energy barriers are ubiquitous for site-pairs located in the 6-MR of CHA. Transition states for Steps S1 and S2 exhibit similar interactions across the 6-MR (Figure 4g,h). Barriers for Steps S1 and S2 at the NNNN site-pair decrease by 3 and 16 kJ mol^{-1} , similar to those on the NNN

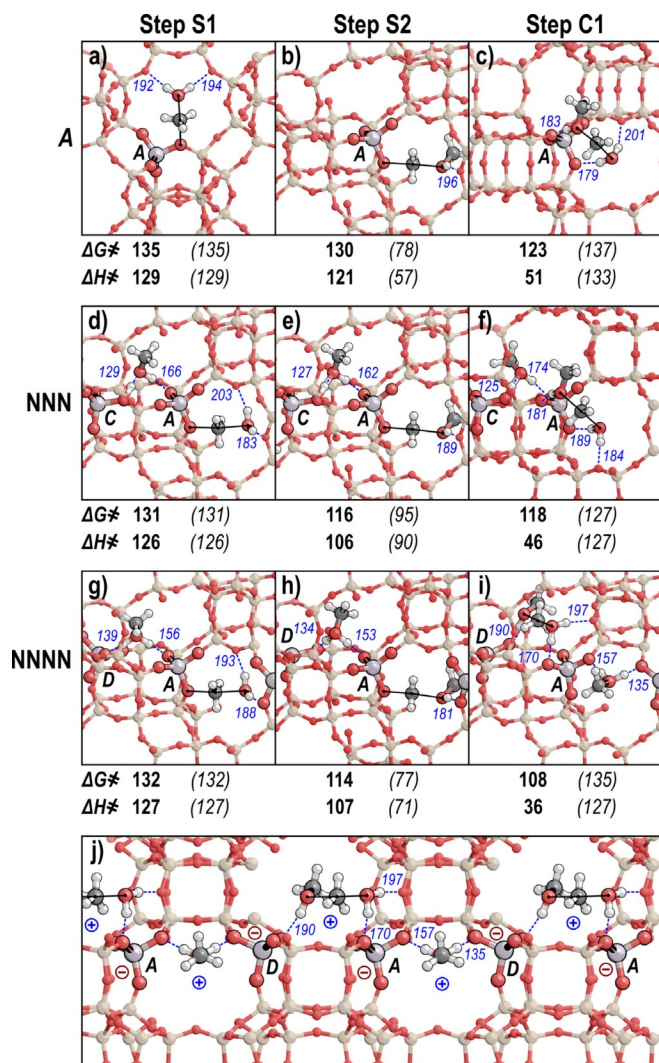


Figure 4. a)–i) The most stable transition state structures for methanol dehydration in CHA for Step S1, Step S2, and Step C1 for isolated acid sites (*A*) and NNN and NNNN site-pairs. Effective free energy (ΔG_{act} and ΔH_{act} in parenthesis and italicized) are in kJ mol^{-1} . Solid black lines indicate incipient and breaking bonds. Blue dashed lines indicate H-bonds (lengths in pm). j) Interactions between alternating cations and anions from periodic boundary conditions in the Step C1 transition state on the NNNN site-pair. Alternate and larger views given for all DFT-obtained structures in Figures S14–S16 (in the Supporting Information).

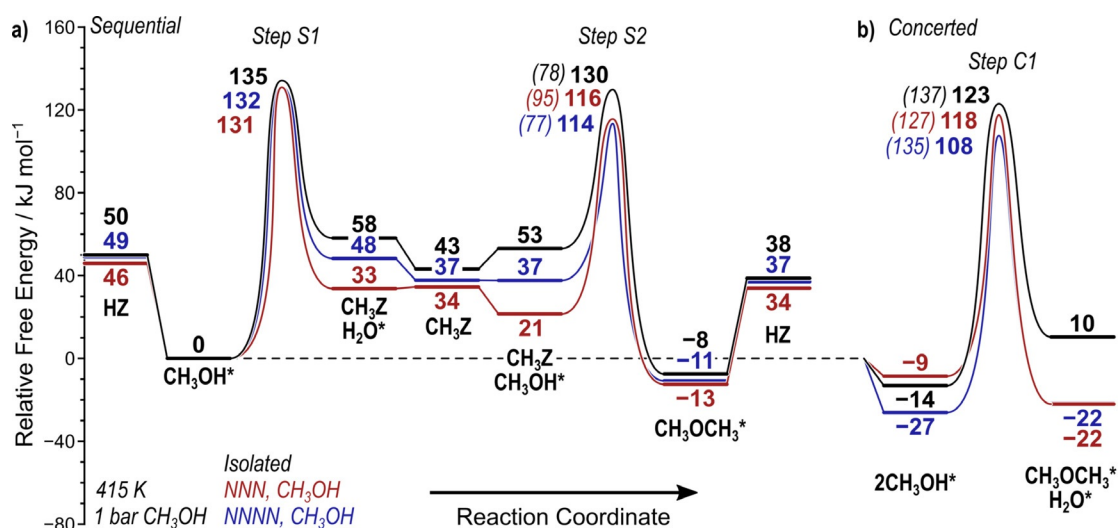


Figure 5. Reaction coordinate diagram for a) sequential and b) concerted methanol dehydration on isolated sites (black), the NNN (red) and NNNN (blue) site-pairs with a CH_3OH monomer at the second acid site. Free energies (415 K, 1 bar) are shown relative to a methanol monomer on all sites. Intrinsic barriers are shown for Steps S2 and C1 in parentheses. Structures for kinetically relevant structures are shown in Figure 4 and Figures S12–S16 in the Supporting Information.

site-pair (Figure 5). The concerted transition state for the NNNN site-pair is unique as it bridges the 6-MR (Figure 4i) while the co-adsorbed methanol interacts simultaneously with the site-pair via the 8-MR(2,4). The simultaneous interaction of this site-pair across the 6-MR and 8-MR(2,4) occurs because of the periodic boundary conditions and the relatively small CHA unit cell. This forms an infinite chain of Al-centered anions and cationic species (Figure 4j), resulting in lower ΔG^\ddagger and ΔG_{act} for the concerted transition state on NNNN site-pairs (108 and 109 kJ mol^{-1}) compared to NNN (118 and 127 kJ mol^{-1}), and again lower than for the isolated site (123 and 138 kJ mol^{-1} , Figure 5). This result indicates that ideal zeolites would have the ability to create long anion-cation chains that stabilize charge-separated transition state structures, like those found in polyphosphobetaines with zwitterionic structures of alternating positive and negative charges in their polymeric chains.^[54,55] Tailored design of such zeolite catalysts, with site-specific high Al content, would confer additional stability to charged transition states; this design motif could apply to any combination of zeolite framework topology and reactions with cationic intermediates, assuming the intermediates are large enough to interact concurrently with nearby sites.

Methanol dehydration barriers are lower on paired sites with co-adsorbed CH_3OH than on isolated sites (Figure 5), but CH_3OH dimers form at higher pressures; therefore, the increases in k_{zero} suggest that similar promotional effects of site-pairing are expected at high CH_3OH coverages. Two co-adsorbed CH_3OH molecules deprotonate Brønsted acid sites to form a protonated dimer complex (Scheme 1).^[22,23,28,37,39,40] When located near the conjugate base of a methanol dehydration transition state, these protonated CH_3OH dimers interact with both deprotonated Al centers simultaneously across the 6-MR (Figure 6). For the prevailing concerted DME formation mechanism, the effective and intrinsic (ΔG^\ddagger

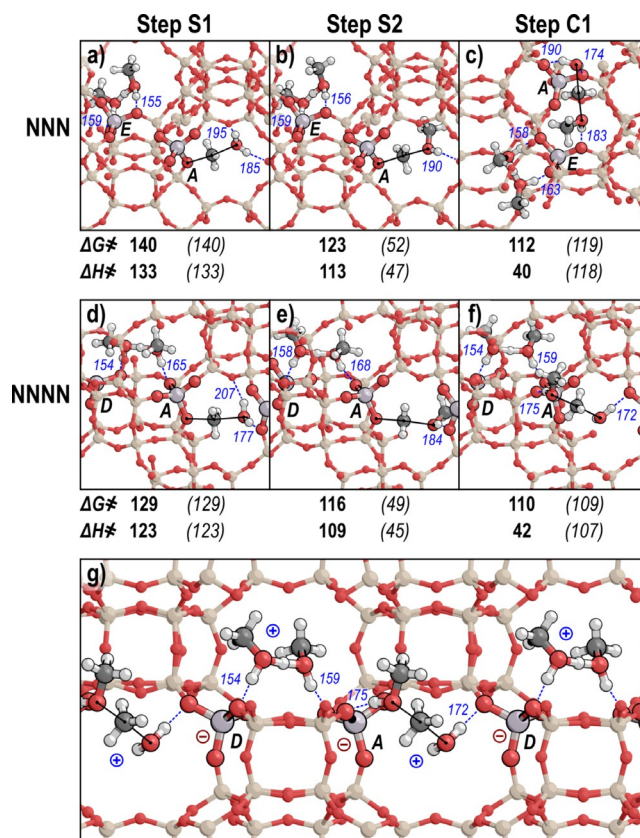


Figure 6. The most stable transition state structures for methanol dehydration in CHA for Step S1, Step S2, and Step C1 for NNN and NNNN site-pairs with protonated methanol dimers on the second site. Effective (ΔG^\ddagger and ΔH^\ddagger) and intrinsic (ΔG_{act} and ΔH_{act} in parenthesis and italicized) are shown in kJ mol^{-1} . Solid black lines indicate incipient and breaking bonds. Blue dashed lines indicate H-bonds (lengths in pm). g) Interactions between alternating cations and anions from periodic boundary conditions in the Step C1 transition state on the NNNN site-pair. Alternate views given in Figures S14–S16 in the Supporting Information.

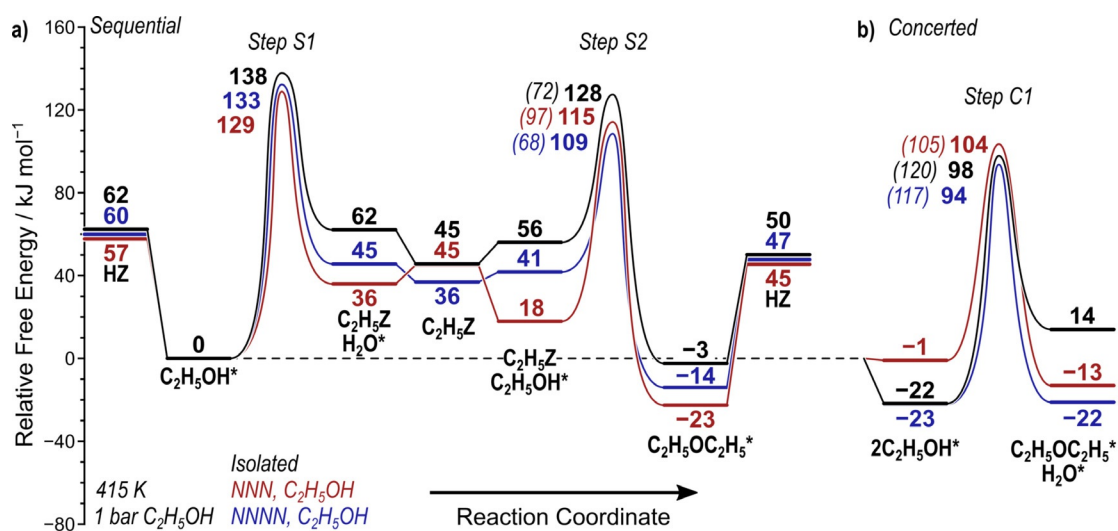


Figure 7. Reaction coordinate diagram for a) sequential and b) concerted ethanol dehydration to diethyl ether (DEE) on isolated sites (black), the NNN site-pair (red), and the NNNN site-pair (blue) with a C₂H₅OH monomer at the second acid site. Free energies (415 K, 1 bar) are shown relative to an ethanol monomer on all sites. Intrinsic barriers are shown for Steps S2 and Step C1 in parentheses. Structures of kinetically relevant states are shown in Figures S21–S25 in the Supporting Information.

and ΔG_{act} barriers are lower (112 and 119 kJ mol⁻¹, Figure 6c) for the NNN site-pair than for isolated sites (123 and 138 kJ mol⁻¹, Figure 4c). Similarly, the NNNN site-pair reduces ΔG^\ddagger and ΔG_{act} by 13 and 29 kJ mol⁻¹, respectively, than those of isolated sites. The “chain” of alternating charges observed in Figure 4j persists here with a cationic CH₃OH dimer above the 6-MR and the cationic bimolecular transition state interacting across the 8-MR(2,4), resulting in lower barriers (Figures 6f and g). Both NNN and NNNN configurations show significant (> 10 kJ mol⁻¹) decreases in the intrinsic barriers (ΔG_{act}) for concerted DME formation even at these higher coverages (4 CH₃OH per CHA cage), once again consistent, if overestimating, the estimated decrease in ΔG_{act} (5 kJ mol⁻¹) obtained by changes in k_{zero} extrapolated from kinetic data.

We further illustrate how proximal sites enhance turnover rates by probing dehydration of a larger alcohol. Ethanol dehydration proceeds via pathways similar to methanol dehydration, but forms diethyl ether (DEE) and water. Ethanol can also dehydrate monomolecularly to form ethylene and water; however, DEE is the primary product formed at the experimental conditions studied here. Paired acid sites ethylate the zeolite with lower barriers (129 and 133 kJ mol⁻¹ for NNN and NNNN, Figure 7) than isolated sites (138 kJ mol⁻¹) because ethanol at the proximal site facilitates an H-bonding interaction that stabilizes the conjugate base (Figure S18, SI), analogous to the methanol case (Figure 4). Effective and intrinsic barriers (ΔG^\ddagger and ΔG_{act}) for concerted DEE formation also decrease from an isolated site ($\Delta G^\ddagger = 98$ kJ mol⁻¹; $\Delta G_{\text{act}} = 120$ kJ mol⁻¹) to an NNNN site-pair ($\Delta G^\ddagger = 94$ kJ mol⁻¹; $\Delta G_{\text{act}} = 117$ kJ mol⁻¹, Figure 7), for which the same interactions that stabilize DME formation transition states prevail. For ethanol dehydration near co-adsorbed ethanol dimers, barriers for the concerted reaction slightly increase for Al in NNN arrangements, but decrease

for Al in NNNN arrangements (Section S10, SI). These DFT data suggest that ethanol dehydration should occur at faster rates on paired than isolated sites in CHA. Indeed, experimental kinetic data show that CHA zeolites with higher percentages of 6-MR paired sites have higher ethanol dehydration turnover rates (per H⁺, Figure 8). Notably, DEE formation on CHA zeolites is not inhibited at high

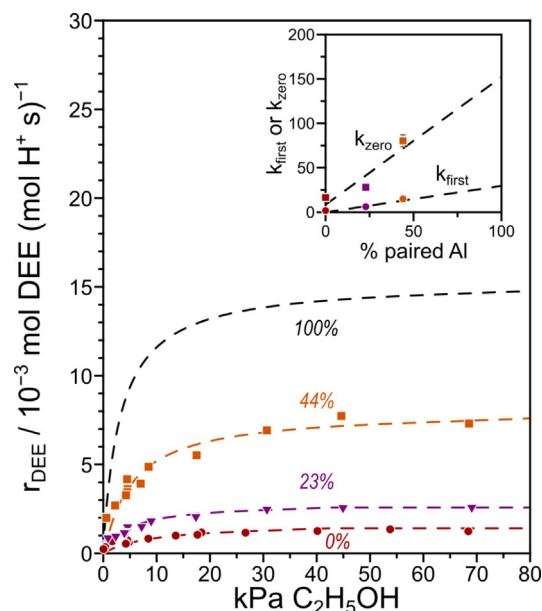


Figure 8. Turnover rate (r_{DEE}) of diethyl ether (DEE) formation (415 K, per H⁺) as a function of ethanol pressure on H-CHA with 0% (●, red), 23% (▼, purple), and 44% (■, orange) of Al in paired configurations. Dashed lines represent regression to Equation (2). Inset: k_{zero} ($10^{-4} \text{ mol DEE} (\text{mol H}^+ \text{ s kPa})^{-1}$) and k_{first} ($10^{-4} \text{ mol DEE} (\text{mol H}^+ \text{ s})^{-1}$) in Equation (2) as functions of the fraction of paired Al.

pressures like methanol,^[28] and the rate of DEE formation is described by:

$$r_{\text{DEE}} = \frac{k_{\text{first}} P_{\text{E}}}{1 + \frac{k_{\text{first}}}{k_{\text{zero}}} P_{\text{E}}} \quad (2)$$

where P_{E} is the ethanol pressure (derivation in Section S11, SI). This indicates that, unlike methanol dehydration, ethanol dehydration transition states are not comprised of more molecules than the MASI at any pressures studied here. Measured first- and zero-order rate coefficients increase by $5 \times$ as 6-MR paired sites increase from 0% to 44% (Figure 8). First- and zero-order rate coefficients [Eq. (2)] fit to the kinetic data predict rate coefficients that are $20 \times$ larger on paired than on isolated sites based on extrapolation to the 100% paired Al limit (Figure 8). These increases in k_{first} and k_{zero} reflect lower effective barriers by 11 and 10 kJ mol^{-1} for first- and zero-order regimes on paired than isolated sites, comparable to differences observed for methanol dehydration between paired and isolated sites.

DFT-calculated free energy barriers indicate that H-bonding interactions between 6-MR paired Al sites stabilize cationic transition state structures more than their reactant precursors, even when those precursors are themselves cationic, resulting in an increase in both first- and zero-order rate coefficients. These interactions between proximal sites are seldom considered, yet often present in Brønsted acid-catalyzed reactions in zeolites, especially at low Si:Al ratios. Critically, we find that such inter-site communication via H-bonding is strengthened by co-adsorbed alkanols compared to a bare proton site (discussed in Section S7, SI), regardless of the size of the alkyl moiety. Such interactions resemble those observed during reactions in zeolites when capillary condensation occurs, wherein intrapore solvents can surround and interact with guest species to alter reaction mechanisms,^[17,56] affect barriers,^[57,58] or stabilize charged intermediates.^[16,59] During alkanol dehydration on paired sites, however, the stabilizing interaction does not require a dense phase, because H-bonding interactions among polar adsorbates enable communication between two proximal Al sites. Zeolite frameworks have long been considered to behave as a pseudo-solvent, given their ability to stabilize reacting intermediates and transition states through non-specific (e.g., dispersive) and specific (e.g., H-bonding) interactions.^[10,43,60–62]

Al centers in the zeolite framework not only generate proton active sites, but also influence the ionic properties of the structured solvent provided by the zeolite framework. Both effects can influence reactivity, just as altering the pH or the ionic strength of a bulk solvent can alter rates of homogeneous reactions.^[63] Al centers in zeolites, however, are held within a rigid crystalline framework, and thus anisotropically position anionic charges in the solvating environment, unlike in liquid phases. Thus, the effect of a spectating Al center depends on its position relative to the active Al center in a zeolite framework. To investigate this in more detail, we consider the case of zeolite methylation at the O3 oxygen of an active site (i.e., Step S1). This step was examined in the absence of co-adsorbed methanol with increasing site density (1–5 Al per unit cell; Si:Al = 35–6.2,

452 total Al arrangements) such that no Al are at NN positions which violate Löwenstein's rule.^[44] An isolated site catalyzes this step with an intrinsic energy barrier ($\Delta E_{\text{S1}}^{\ddagger}$) of 122 kJ mol^{-1} (Figure 9). Among the 23 different two-Al configurations examined, $\Delta E_{\text{S1}}^{\ddagger}$ varies from 106 to 128 kJ mol^{-1} , representing a decrease of up to 16 kJ mol^{-1} or an increase of up to 6 kJ mol^{-1} compared to the isolated Al case (Figure 9). Importantly, these barriers do not correlate with any simple geometric descriptor such as Al-Al distance or Al-C distance (Figure S29, SI); instead, proximal Al centers placed in specific arrangements can either raise or lower barriers. For example, Al placed across 4-MR structures from the reacting site increase barriers (consistent with weaker acids predicted by DPE for such arrangements),^[21] while those placed across 6- or 8-MR structures generally lower barriers (Figure S31, SI).

With each addition of a proximal site, barriers shift by as much as $\pm 37 \text{ kJ mol}^{-1}$, resulting in barriers as low as

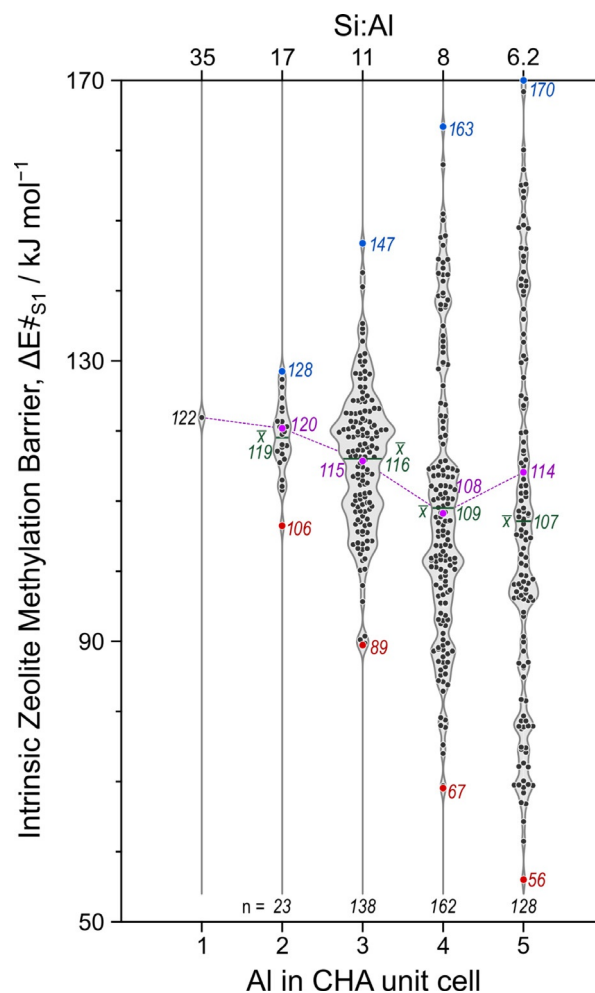


Figure 9. Intrinsic potential energy barriers ($\Delta E_{\text{S1}}^{\ddagger}$) for zeolite methylation (Step S1) occurring on O3 of the A site with 1–5 Al in the CHA unit cell (Si:Al = 6.2–35). For each Al content, the minimum (red), maximum (blue), average (\bar{x} , green), and effective (purple, assuming Al occupy sites according to a Boltzmann distribution at 415 K) barriers are labeled, along with the total number of Al arrangements studied (n ; discussed in Section S12 in the Supporting Information).

56 kJ mol⁻¹ or as high as 170 kJ mol⁻¹ (Figure 9; Si:Al = 6.2). These shifts in barriers are nearly symmetric, such that the average barrier decreases slightly to 107 kJ mol⁻¹ at the highest Al content (Figure 9). If Al are assumed to be distributed thermodynamically (i.e., based on a Boltzmann average), then the effective barrier can be computed for each Si:Al ratio. This Boltzmann-averaged barrier decreases nearly monotonically as Al content increases, to a minimum of 108 kJ mol⁻¹ at Si:Al of 8 and 114 kJ mol⁻¹ at Si:Al of 6.2 (Figure 9). These spectating Al are not directly involved in the methylation transition state; rather, they modify the solvation environment provided by the zeolite by altering its polarity and providing H-bonding sites that interact with the transition state or conjugate base of the reacting site, in a manner sensitive to the specific positions of the Al centers, resulting in dramatic effects (both increases and decreases) in activation barriers.

Conclusion

DFT calculations and experimental kinetic and spectroscopic data reveal that altering the proximity and arrangement of framework Al and their associated Brønsted acid sites modifies the solvating environments of zeolite pores, by altering their polarity and H-bonding capacity, so as to significantly increase or decrease activation barriers for zeolite-catalyzed reactions. These shifts in barriers cannot be predicted by Al-Al distances or Al densities alone, but depend strongly on the specific locations of spectating Al centers. For example, Al located across 4-MR in CHA generally result in weaker acids and higher activation barriers, whereas Al located across 6-MR or at certain 8-MR positions decrease activation barriers. Alkanol dehydration rates are enhanced on paired sites located in 6-MR of CHA, because H-bonding interactions are facilitated by co-adsorbed alkanols that stabilize the conjugate base of reacting sites to lower barriers. Such inter-site cooperation is distinct from that observed in dense intrapore phases, wherein solvent species act as proton shuttles or interact with co-adsorbates,^[17] rather, these H-bonding interactions are mediated by co-adsorbed reactants without an intermediary solvent phase, thus requiring Al sites to be positioned in specific locations to accommodate the geometric limitations imposed by the size and structure of the reactant complex and the connecting H-bonds. Such interactions are likely sensitive to the topology of the zeolite framework; thus, these findings on CHA are expected to hold for small-pore zeolite frameworks with similar 6- and 8-MR motifs (e.g., LTA, AEI), but extending these conclusions to zeolites characterized by different topological features (e.g. MFI) requires further investigation. Additionally, our results indicate that further barrier reductions can occur with chains of alternating cationic and anionic charges that mimic long chains of alternating charges in some zwitterionic polymers.^[54,55] These mechanistic insights into the specific interactions of proximal binding sites and co-adsorbates during Brønsted acid-catalyzed reactions in zeolites have gone previously unrecognized, and provide new targets for synthesizing zeolites with framework Al arrangements

tailored to match the geometries of reactants and transition states to maximize H-bonding among these moieties.

Acknowledgements

A.H., S.N., and D.H. acknowledge financial support from the ACS Petroleum Research Fund New Doctoral Investigation Award (57079DNI5) and the National Science Foundation CAREER program (1942684-CBET). This work used the Extreme Science and Engineering Discovery Environment (XSEDE),^[64] which is supported by the National Science Foundation grant number ACI-1548562 through allocation CTS160041. J.B., J.D.I., C.N., and R.G. acknowledge financial support by the National Science Foundation DMREF program (1922173-CBET) for the experimental work at Purdue.

Conflict of interest

The authors declare no conflict of interest.

Keywords: alkanol dehydration · DFT calculations · heterogeneous catalysis · solvation · zeolites

- [1] A. Corma, *Chem. Rev.* **1995**, *95*, 559–614.
- [2] W. Vermeiren, J. P. Gilson, *Top. Catal.* **2009**, *52*, 1131–1161.
- [3] M. E. Davis, *Nature* **2002**, *417*, 813–821.
- [4] M. Choi, H. S. Cho, R. Srivastava, C. Venkatesan, D.-H. Choi, R. Ryoo, *Nat. Mater.* **2006**, *5*, 718–723.
- [5] A. I. Lupulescu, J. D. Rimer, *Angew. Chem. Int. Ed.* **2012**, *51*, 3345–3349; *Angew. Chem.* **2012**, *124*, 3401–3405.
- [6] M. Moliner, C. Martínez, A. Corma, *Angew. Chem. Int. Ed.* **2015**, *54*, 3560–3579; *Angew. Chem.* **2015**, *127*, 3630–3649.
- [7] C. Jo, J. Jung, H. S. Shin, J. Kim, R. Ryoo, *Angew. Chem. Int. Ed.* **2013**, *52*, 10014–10017; *Angew. Chem.* **2013**, *125*, 10198–10201.
- [8] E. M. Gallego, M. T. Portilla, C. Paris, A. León-Escamilla, M. Boronat, M. Moliner, A. Corma, *Science* **2017**, *355*, 1051–1054.
- [9] R. Gounder, E. Iglesia, *Angew. Chem. Int. Ed.* **2010**, *49*, 808–811; *Angew. Chem.* **2010**, *122*, 820–823.
- [10] R. Gounder, E. Iglesia, *Chem. Commun.* **2013**, *49*, 3491–3509.
- [11] E. G. Derouane, M. E. Davis, *J. Mol. Catal.* **1988**, *48*, 37–41.
- [12] B. C. Bukowski, J. S. Bates, R. Gounder, J. Greeley, *Angew. Chem. Int. Ed.* **2019**, *58*, 16422–16426; *Angew. Chem.* **2019**, *131*, 16574–16578.
- [13] M. A. Mellmer, C. Sener, J. M. R. Gallo, J. S. Luterbacher, D. M. Alonso, J. A. Dumesic, *Angew. Chem. Int. Ed.* **2014**, *53*, 11872–11875; *Angew. Chem.* **2014**, *126*, 12066–12069.
- [14] M. A. Mellmer, C. Sanpitakseree, B. Demir, P. Bai, K. Ma, M. Neurock, J. A. Dumesic, *Nat. Catal.* **2018**, *1*, 199–207.
- [15] S. Eckstein, P. H. Hintermeier, R. Zhao, E. Baráth, H. Shi, Y. Liu, J. A. Lercher, *Angew. Chem. Int. Ed.* **2019**, *58*, 3450–3455; *Angew. Chem.* **2019**, *131*, 3488–3493.
- [16] M. Wang, N. R. Jaegers, M.-S. Lee, C. Wan, J. Z. Hu, H. Shi, D. Mei, S. D. Burton, D. M. Camaioni, O. Y. Gutiérrez, et al., *J. Am. Chem. Soc.* **2019**, *141*, 3444–3455.
- [17] G. Li, B. Wang, D. E. Resasco, *ACS Catal.* **2020**, *10*, 1294–1309.
- [18] J. S. Bates, B. C. Bukowski, J. Greeley, R. Gounder, *Chem. Sci.* **2020**, *11*, 7102–7122.
- [19] B. C. Knott, C. T. Nimlos, D. J. Robichaud, M. R. Nimlos, S. Kim, R. Gounder, *ACS Catal.* **2018**, *8*, 770–784.
- [20] J. Dědeček, Z. Sobalík, B. Wichterlová, *Catal. Rev.* **2012**, *54*, 135–223.

- [21] S. Nystrom, A. Hoffman, D. Hibbitts, *ACS Catal.* **2018**, *8*, 7842–7860.
- [22] A. J. Jones, R. T. Carr, S. I. Zones, E. Iglesia, *J. Catal.* **2014**, *312*, 58–68.
- [23] R. T. Carr, M. Neurock, E. Iglesia, *J. Catal.* **2011**, *278*, 78–93.
- [24] C. Song, Y. Chu, M. Wang, H. Shi, L. Zhao, X. Guo, W. Yang, J. Shen, N. Xue, L. Peng, et al., *J. Catal.* **2017**, *349*, 163–174.
- [25] A. N. Mlinar, P. M. Zimmerman, F. E. Celik, M. Head-Gordon, A. T. Bell, *J. Catal.* **2012**, *288*, 65–73.
- [26] M. Bernauer, E. Tabor, V. Pashkova, D. Kaucký, Z. Sobalík, B. Wichterlová, J. Dedecek, *J. Catal.* **2016**, *344*, 157–172.
- [27] E. Tabor, M. Bernauer, B. Wichterlová, J. Dedecek, *Catal. Sci. Technol.* **2019**, *9*, 4262–4275.
- [28] J. R. Di Iorio, A. J. Hoffman, C. T. Nimlos, S. Nystrom, D. Hibbitts, R. Gounder, *J. Catal.* **2019**, *380*, 161–177.
- [29] C. Baerlocher, L. B. McCusker, D. H. Olson, *Atlas of zeolite framework types*, Elsevier, Amsterdam, **2007**.
- [30] J. R. Di Iorio, R. Gounder, *Chem. Mater.* **2016**, *28*, 2236–2247.
- [31] J. R. Di Iorio, S. Li, C. B. Jones, C. T. Nimlos, Y. Wang, E. Kunkes, V. Vattipalli, S. Prasad, A. Moini, W. F. Schneider, et al., *J. Am. Chem. Soc.* **2020**, *142*, 4807–4819.
- [32] J. R. Di Iorio, C. T. Nimlos, R. Gounder, *ACS Catal.* **2017**, *7*, 6663–6674.
- [33] A. Janda, A. T. Bell, *J. Am. Chem. Soc.* **2013**, *135*, 19193–19207.
- [34] M. Zeets, D. E. Resasco, B. Wang, *Catal. Today* **2018**, *312*, 44–50.
- [35] V. Pashkova, P. Klein, J. Dedecek, V. Tokarová, B. Wichterlová, *Microporous Mesoporous Mater.* **2015**, *202*, 138–146.
- [36] M. D. Oleksiak, K. Muraoka, M.-F. Hsieh, M. T. Conato, A. Shimojima, T. Okubo, W. Chaikittisilp, J. D. Rimer, *Angew. Chem. Int. Ed.* **2017**, *56*, 13366–13371; *Angew. Chem.* **2017**, *129*, 13551–13556.
- [37] A. J. Jones, E. Iglesia, *Angew. Chem. Int. Ed.* **2014**, *53*, 12177–12181; *Angew. Chem.* **2014**, *126*, 12373–12377.
- [38] R. Gounder, A. J. Jones, R. T. Carr, E. Iglesia, *J. Catal.* **2012**, *286*, 214–223.
- [39] A. Ghorbanpour, J. D. Rimer, L. C. Grabow, *ACS Catal.* **2016**, *6*, 2287–2298.
- [40] P. G. Moses, J. K. Nørskov, *ACS Catal.* **2013**, *3*, 735–745.
- [41] T. J. Wilke, M. A. Barteau, *J. Catal.* **2019**, *371*, 357–367.
- [42] P. Deshlahra, R. T. Carr, E. Iglesia, *J. Am. Chem. Soc.* **2014**, *136*, 15229–15247.
- [43] A. J. Jones, S. I. Zones, E. Iglesia, *J. Phys. Chem. C* **2014**, *118*, 17787–17800.
- [44] W. Löwenstein, *Am. Mineral.* **1954**, *39*, 92–96.
- [45] R. Gounder, E. Iglesia, *J. Am. Chem. Soc.* **2009**, *131*, 1958–1971.
- [46] R. Gounder, E. Iglesia, *J. Catal.* **2011**, *277*, 36–45.
- [47] A. Bhan, R. Gounder, J. Macht, E. Iglesia, *J. Catal.* **2008**, *253*, 221–224.
- [48] A. Janda, B. Vlaisavljevich, L.-C. Lin, B. Smit, A. T. Bell, *J. Am. Chem. Soc.* **2016**, *138*, 4739–4756.
- [49] F. C. Jentoft, B. C. Gates, *Top. Catal.* **1997**, *4*, 1–13.
- [50] C.-J. Chen, S. Rangarajan, I. M. Hill, A. Bhan, *ACS Catal.* **2014**, *4*, 2319–2327.
- [51] S. Schallmoser, T. Ikuno, M. F. Wagenhofer, R. Kolvenbach, G. L. Haller, M. Sanchez-Sanchez, J. A. Lercher, *J. Catal.* **2014**, *316*, 93–102.
- [52] S. Mallikarjun Sharada, P. M. Zimmerman, A. T. Bell, M. Head-Gordon, *J. Phys. Chem. C* **2013**, *117*, 12600–12611.
- [53] M. DeLuca, P. Kravchenko, A. Hoffman, D. Hibbitts, *ACS Catal.* **2019**, *9*, 6444–6460.
- [54] A. Laschewsky, *Polymers* **2014**, *6*, 1544–1601.
- [55] S. Kudaibergenov, W. Jaeger, A. Laschewsky, *Supramolecular polymers polymeric betains oligomers*, Springer Berlin Heidelberg, Berlin, **2006**, pp. 157–224.
- [56] Y. Liu, E. Baráth, H. Shi, J. Hu, D. M. Camaioni, J. A. Lercher, *Nat. Catal.* **2018**, *1*, 141–147.
- [57] D. T. Bregante, A. M. Johnson, A. Y. Patel, E. Z. Ayla, M. J. Cordon, B. C. Bukowski, J. Greeley, R. Gounder, D. W. Flaherty, *J. Am. Chem. Soc.* **2019**, *141*, 7302–7319.
- [58] M. J. Cordon, J. W. Harris, J. C. Vega-Vila, J. S. Bates, S. Kaur, M. Gupta, M. E. Witzke, E. C. Wegener, J. T. Miller, D. W. Flaherty, et al., *J. Am. Chem. Soc.* **2018**, *140*, 14244–14266.
- [59] A. Vjunov, M. Wang, N. Govind, T. Huthwelker, H. Shi, D. Mei, J. L. Fulton, J. A. Lercher, *Chem. Mater.* **2017**, *29*, 9030–9042.
- [60] E. G. Derouane, *J. Mol. Catal. A* **1998**, *134*, 29–45.
- [61] M. L. Sarazen, E. Doskocil, E. Iglesia, *ACS Catal.* **2016**, *6*, 7059–7070.
- [62] M. L. Sarazen, E. Doskocil, E. Iglesia, *J. Catal.* **2016**, *344*, 553–569.
- [63] P. J. Dyson, P. G. Jessop, *Catal. Sci. Technol.* **2016**, *6*, 3302–3316.
- [64] J. Towns, T. Cockerill, M. Dahan, I. Foster, K. Gaither, A. Grimshaw, V. Hazlewood, S. Lathrop, D. Lifka, G. D. Peterson, et al., *Comput. Sci. Eng.* **2014**, *16*, 62–74.

Manuscript received: June 3, 2020

Accepted manuscript online: July 13, 2020

Version of record online: August 26, 2020